Multidisciplinary Approaches for Studying and Combating Microbial Pathogens

Edited by

A. Méndez-Vilas

BrownWalker Press
Boca Raton

Multidisciplinary Approaches for Studying and Combating Microbial Pathogens

BrownWalker Press
Boca Raton, Florida • USA
2015

ISBN-10: 1-62734-544-2
ISBN-13: 978-1-62734-544-6

www.brownwalker.com

Cover image by Eraxion/Bigstock.com

TABLE OF CONTENTS

Introduction

We are pleased to present a selection of papers presented at The III International Conference on Antimicrobial Research (ICAR2014), which was held in Madrid, Spain, from 1 to 3 October 2014.

The aims of this conference were to provide a forum for discussion of cutting edge antimicrobial research and to create an opportunity for microbiologists, biochemists, genetists, clinicians, physicists, engineers… to meet and have the chance to find new research colleagues and partners for future research works. This third edition gathered 444 participants, coming from 58 countries, and nearly 450 works were presented at the conference. Some of those research works are discussed in this book covering the topics: antimicrobial natural products, biofilms, antimicrobial surfaces, antimicrobial resistance and clinical and medical microbiology…

We would like to thank the International Advisory Committee of this conference, a group of international experts who guided us in the development of the conference program. And, of course, we also thank the authors for submitting their work and sharing their findings.

This book serves as formal proceedings of the meeting. We hope readers will find this set of papers inspiring and stimulating in their current research work and look forward to seeing another fruitful edition in 2016.

A. Méndez-Vilas
Editor
ICAR2014 General Coordinator

A clinical resistant isolate of opportunistic fungal pathogen, *Candida albicans* revealed more rigid membrane than its isogenic sensitive isolate

Arvind Kumar[1,€], V. S. Radhakrishnan[1,€], Richa Singh[1], Manish Kumar[1], Nagendra N. Mishra[2] and **Tulika Prasad[1,*]**

[1]Advanced Instrumentation Research Facility (AIRF), Jawaharlal Nehru University, New Delhi-110067, India.
[2]Staph Membrane Lab, Infectious Diseases, LABiomed, Harbor- UCLA Medical Center, Torrance, USA.
[€]Both authors contributed equally to this work.
*Corresponding author email: prasadtulika@hotmail.com; prasadtulika@mail.jnu.ac.in

The opportunistic dimorphic fungal pathogen, *Candida albicans* is among the top five most common causes of global nosocomial infections leading to almost 40% mortality and morbidity in immunocompromised patients. Increasing incidence of multidrug resistant strains has emerged as a significant threat to the treatment of *Candidiasis*.

The fundamental physical properties of the cell membrane are strongly linked with their biological functions. Membrane provides a permeability barrier to the entry of biomolecules across the cell. It is extremely interesting to investigate the key role played by membrane fluidity in regulating the drug resistance observed in the clinical microbial strains. This study has been carried out to characterize the changes in the membrane fluidity in different phases of growth which includes the lag phase, log phase and stationary phase of cells in an isogenic pair of clinical isolate (GU4-sensitive; GU5-resistant) of *Candida albicans*. Microviscosity of membrane has been measured in this study using fluorescence polarization and the probe, 1, 6-Diphenyl 1, 3, 5-hexatriene (DPH). The reciprocal of fluidity (Micro-viscosity) is the measure of fractional resistance to rotational and translational motion of molecule. With changes in growth phase from lag to log phase, the resistant isolate GU5 was found to attain a more rigid membrane than the sensitive isolate GU4 but after log phase it appeared that the equilibrium is achieved during stationary phase for membrane fluidity for the two isolates and they attain identical physical state of the membrane. Therefore, increased rigid behavior of membrane may be responsible for reduction in passive drug diffusion for the resistant isolate in log phase and at the same time, it also appeared that both the isolates attained a steady state of equilibrium during the stationary phase adapting to the changes in physical state of the membrane. GU5 showed overexpression of the ABC pump membrane protein CDR1p which may be attributed to the observed differences in their membrane fluidity. Membrane fluidity is a parameter of the physical state of the membrane which largely affects the passive diffusion of the drugs and hence the observed resistance towards drugs. The resistance towards drugs also appeared to be influenced by the host environment, prior exposure to drugs and overexpression of different drug efflux pump proteins. The *Candida* cells appeared to adapt to changes in the environment through modulation of their membrane properties and lipid composition leading to altered membrane fluidity.

Keywords: *Candida albicans*; drug resistance; membrane fluidity; isogenic clinical isolates; ABC pump protein

1. Introduction

The burden of antifungal resistance has emerged as a major concern of global public health. There has been a dramatic increase since 1970s in the number of immunocompromised individuals associated with increased usage of immunosuppressive therapies and since 1980s in the prevalence of fungal diseases due to AIDS [1].*Candida* infections have been reported to significantly affect human health and attribute to high mortality rates [2]. *Candida* spp. are polymorphic, opportunistic fungi normally residing in the human microbiome as benign, commensal organisms accounting for 75% of the population. However, under immunocompromised conditions, their pathogenic potential is triggered to cause infections ranging from superficial to life threatening systemic mycoses [3]. *Candida spp.* especially *Candida albicans* ranks as the fourth most common cause of hospital acquired infection among immunocompromised individuals causing bloodstream infections with mortality rate ranging between 38 to 49 % [4, 5]. Antifungal agents, such as azoles and echinocandins have played an important role in the treatment of *Candida* infections [1, 6]. In recent years, efforts have been made to overcome emergence of drug resistant fungi by using drug combinations but high cost and serious side effects have limited such combinatorial therapy [6].

Availability of fewer antifungals puts a constraint to the clinicians' therapeutics which gets further narrowed down by the emergence of drug resistance/ azole resistant strains [7, 8]. Drug tolerance may be an immediate manifestation of response of the organism to drugs leading to subsequent development of drug resistance [8]. Acquisition of multi drug resistance (MDR) may be due to multitude of factors as shown in Fig. 1 which includes i) drug target alteration (by point mutation, overexpression and gene amplification), ii) modification and degradation of drug, iii) increased drug extrusion (by overexpression of drug efflux pumps) and/or iv)

decreased drug import or altered intracellular drug accumulation (by altered physical state of the membrane and altered permeability) [7, 8]. Membrane functions may be influenced by factors such as lipid composition, membrane order, lipid asymmetry and glycosylation. Clinical drug resistance is thus multifactorial and may be attributed to a combination of factors related to the host environment, antifungal compounds and pathogen biology. In order to develop an efficient and quick treatment and improved outcome of systemic mycoses, it is essential to have a better understanding of the mechanisms and clinical impact of drug resistance [7, 8].

In addition to the common mechanisms of drug resistance frequently studied, it is important to study changes in structure and function of cell membrane between sensitive and resistant isolates (with prolonged exposure to drugs) for fully elucidating the mechanism of development of drug resistance. This study is an effort to characterize the membrane biophysical state and its possible role in clinical drug resistance for a pair of matched isolates (isogenic) for *Candida albicans*, obtained from the same AIDS patient with recurrent episodes of orophrayngeal *Candidasis* (OPC) and which became fluconazole resistant during therapy [9]. Correlation between resistance and alterations in membrane biophysical properties of the sensitive and resistant *Candida* isolates has been elucidated in this study by using environment-sensitive fluorescent probe, 1, 6-Diphenyl 1, 3, 5-hexatriene (DPH).

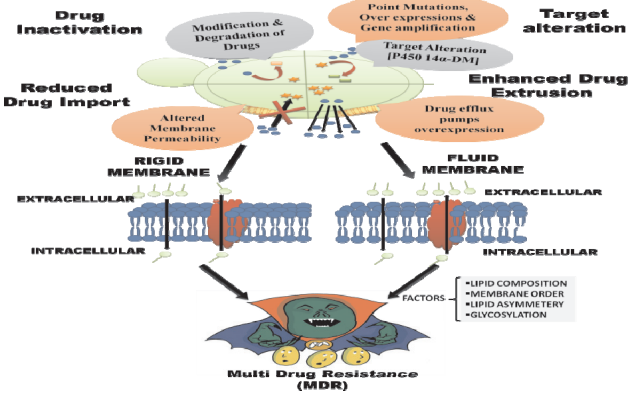

Fig. 1: Molecular mechanisms of fungal multi drug resistance

2. Materials and methods

2.1 Materials, Strains, Media and Growth Conditions

Analytical grade chemicals and HPLC grade solvents used for this study were obtained from HI-Media (Mumbai, India) and Fisher Scientific (Mumbai, India). Lyticase, DPH, tetrahydrofuran (THF) and antifungal drugs viz. fluconazole, itraconazole, ketoconazole, terbinafine were procured from Sigma Chemicals Aldrich (St. Louis, Mo., USA). Table 1 lists the strains used for this study. Cells grown on YEPD (1% Yeast Extract, 2% Peptone, and 2% D-glucose) at 30°C were used for all experiments.

Table 1: Description of strains used for this study

Strain Name	Strain Description
SC5314	Wild type [10]
GU4	Fluconazole sensitive strain with low levels of *CDR1/2* mRNA [9]
GU5	Fluconazole resistant strain with high levels of *CDR1/2* mRNA [9]

2.2 Minimum Inhibitory Concentration (MIC) determination

MIC was determined by broth micro-dilution method as described earlier [11, 12] in accordance with the recommendations of the Clinical and Laboratory (CLSI), formerly National Committee for the Clinical Laboratory Standards (NCCLS).A drug free control was also included. The following concentrations of stock solution of drugs along with their respective solvents (given in parentheses) were used: fluconazole 5mg/ml (DMSO); ketoconazole 1mg/ml (DMSO); itraconazole 1mg/ml (DMSO) and terbinafine 1mg/ml (Ethanol).

2.3 Assessing the physical state of the membrane

Membrane fluidity of cell membrane was monitored using fluorescent probe, DPH as described earlier [11, 13, 14] with slight modifications. Spheroplasts were prepared using lyticase enzyme at 30°C for 3-4 hrs. The spheroplasts were resuspended in labelling buffer pH 7.4 (0.6M Sorbitol, 10mM $MgSO_4$ and 20mM Tris-Cl) and incubated with 2µm DPH for 1hr at 30°C. Fluorescence polarization (p) was calculated as follows on Perkin-Elmer LS55 spectrofluorimeter (excitation 360 nm, emission 426 nm, slit size for both excitation and emission 10 nm) [15]:

$$p = \frac{I_{VV} - (I_{VH} \times G)}{I_{VV} + (I_{VH} \times G)}$$

Where, I_{VV} = Corrected fluorescence intensity obtained with excitation by vertically polarized light and emission detected by analyzer oriented vertically to the direction of polarized excitation light, I_{VH} = Corrected fluorescence intensity obtained with excitation by vertically polarized light and emission detected by analyzer oriented horizontal to the direction of polarized excitation light. *Grating Factor G*, correction for optical components is calculated as I_{HV}/I_{HH} where subscripts HV and HH indicate corrected fluorescence intensity values obtained with horizontal-vertical orientation and horizontal-horizontal orientation for the polarizer and analyzer in that order respectively.

The time resolved fluorescence decay for DPH (excitation 360 nm and emission at 426 nm) was monitored for the above labelled cells in Edinburgh FL920 Fluorescence Life Time Spectrometer as described elsewhere [16].

2.4 Study of ultrastructure of the cells using Transmission Electron Microscopy (TEM)

TEM was used to study the cellular ultrastructure of the clinical isolates. YEPD grown cells were harvested, PBS washed and fixed with 2.5% glutaraldehyde for 2-3 hours at room temperature (RT) and 4-5 hours at 4°C. Cells were then washed 3-4 times with PBS and dehydrated with graded acetone, cleared with toluene and then infiltrated with toluene and araldite mixture at RT. Samples were put overnight in pure araldite at 50°C and then embedded in 1.5 ml eppendorf tube at 60°C. Semi thin and ultrathin sections cut with ultra-microtome (Ultra-microtome Leica EM UC6) were taken on 3.05 mm diameter and 200 mesh copper grid, stained with uranyl acetate and subsequently observed at 120 kV under TEM (Model name JEOL2100F with Accelerating Voltage 80kV-200kV and Magnification 50 to 1,500,000X).

3. Results & Discussion

Isogenic/ matched pair of clinical isolates (GU4-sensitive and GU5-resistant) collected from same AIDS patient, which became fluconazole resistant during therapy were used for this study along with wild type SC5314. MIC_{90} (µg/ml) (Table 2) confirmed the MDR phenotype for GU5. Highest MIC was observed for GU5 for fluconazole, ketoconazole, itraconazole and terbinafine whereas SC5314 and GU4 showed sensitivity towards these drugs. GU4 showed a relatively higher MIC for all drugs than SC5314 which may be largely due to their prior exposure to drug and complex host factors in the human patient.

Table 2: MIC_{90} for different drugs for Wild type (SC5314) and clinical isolates (GU4 and GU5)

Strain Name	**MIC $_{90}$ in µg/ml**			
	Fluconzaole	**Itraconazole**	**Ketoconazole**	**Terbinafine**
SC5314	3.125	0.015	0.062	3.06
GU4	6.25	0.031	0.125	6.125
GU5	>200	1	>2	12.25

Cell envelope serves as a barrier for entry or exit of biomolecules across the cells. Many cellular changes with different structure, function and mechanism may accompany the drug resistance phenotype which may be intrinsic (inherent) or acquired. As an effort to study the multitude of factors involved in acquiring clinical resistance, membrane biophysical properties for the sensitive and resistant isolates were analyzed in this study at different phases of growth using fluorescence polarization. *Candida* cells showed a typical sigmoid growth pattern (Fig. 2A) with early lag phase till 6 hours, lag phase till 10 hours, early log phase at 12 hours, log/ exponential phase between 14-18 hours and approaching stationary phase 20 hours onwards.

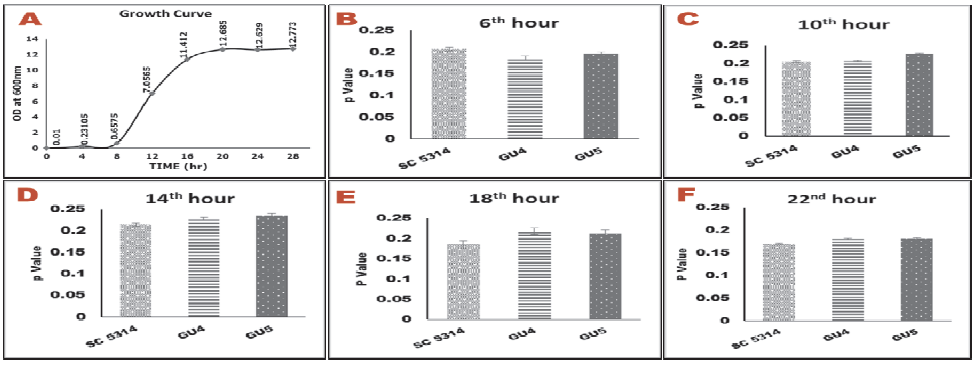

Fig. 2: (A) Growth curve of *Candida* cells. **(B-F)** Mean fluorescence polarization "p" values (inversely proportional to membrane fluidity) ± the standard deviation of the mean of the three sets of experiments, of wild type (SC5314) and clinical isolates (GU4 and GU5) at different hours of growth.

Sterol rich membrane microdomains have been reported to exist in eukaryotes and play a crucial role in membrane structure, organization and function. Sterols and specific lipids have been found to be non-randomly distributed in such domains of biological membranes [17]. Fluorescence being sensitive to the cellular physicochemical environment, DPH was used to study organizational dynamics of the hydrophobic interior of the membrane in the sensitive and resistant isolates. Statistically significant differences were observed between them at different phases of growth by steady state fluorescence polarization and time resolved fluorescence measurements (Fig. 2B-F and Table 3). Packing of sterol and fatty acyl chain is likely to affect the diffusion rate of membrane embedded probes, thus affecting fluorescence polarization values. Fluorescence polarization is inversely proportional to membrane fluidity and increase in fluorescence polarization values are typically due to a reduction in rotational mobility of the fluorophore, which is influenced by dense packing of membrane. GU5 showed increase in membrane rigidity than its sensitive pair GU4 with increase in hours of growth and fluorescence polarization values increased in GU5 by 4.43% (6 hours), 8.44% (10 hours) and 3.77% (14 hours). No significant differences were observed between the two isolates at 18 hours and 22 hours of growth and fluorescence polarization values in GU5 decreased by only 2.06% (18 hours) and increased by 0.5 % (22 hours). Wild type SC5315 in absence of prior exposure to host factors showed different behaviour than the clinical pair i.e. higher rigidity at 6 hour of growth and from 10 hour onwards revealed higher fluidity than the other two clinical isolates. The observed results may be due to differences in the levels of compaction of cell membrane between sensitive and resistant isolates and differences in lateral organization on the plane of membrane contributed by ergosterol, sphingolipids and overexpressed drug efflux pump proteins.

Fluorescence lifetime is a reliable indicator of polarity changes in local environment of the DPH. Life time of DPH has been found to be reduced in presence of water in its immediate environment [17]. The mean fluorescent lifetimes (Table 3) were calculated from the fitting of tri-exponential fluorescent decay curves [16]. The data revealed that DPH lifetime for the resistant isolate is always lower than the sensitive isolate and the decay for DPH becomes faster with increase in time of growth from 6 to 22 hours. The sensitive isolate shows gradual lowering of decay time of DPH from 6 hours to 18 hour of growth and increases again at 22 hours of growth in sensitive isolate. Increase in water penetration might have increased the polarity of the environment resulting in shortening of DPH lifetime. Previous reports mention that ergosterol beyond a certain concentration do not influence dynamics and membrane order [17]. Water penetration may be more due to lesser rigidifying effect of ergosterol as revealed by fluorescence polarization. These decay patterns provided the observed changes in the cellular microenvironment of the respective membrane during different phases of growth.

Table 3: Lifetime decay for DPH in nanoseconds (ns) at different hours of growth for the clinical isolates (GU4 and GU5)

Strains Name	6th Hour (ns)	10th Hour (ns)	14th hour (ns)	18th Hour (ns)	22nd Hour (ns)
GU4	2.8	1.9	0.94	0.75	1.12
GU5	2.24	1	0.68	0.57	0.73

It is evident that with changes in growth phase from lag to log phase, the resistant isolate GU5 attained a more rigid membrane than the sensitive isolate GU4 but after log phase it appeared that equilibrium was achieved for membrane fluidity. This data indicated that membranes of the clinically resistant isolate (GU5) exhibited rigidity favouring the development of drug resistance. Rigid behaviour of membrane is likely to show reduction in passive drug diffusion. At the same time, all isolates appeared to attain a steady state of equilibrium

during the stationary phase adapting to the changes in physical state of the membrane. It may be noted that GU5 showed overexpression of the ABC pump membrane proteins CDR1/2p [9].

There are reports suggesting involvement of ultrastructural changes in the cell envelope in development of drug resistance which includes increase in cell wall thickness [18]. Although the changes observed in membrane order were dependent on the cellular microenvironment, thickening of cell wall was consistently observed with increase in clinical resistance. The cell wall thickness was in the order: wild type SC5314 (74.6 nm) < sensitive GU4 (90.3 nm) < resistant GU5 (117nm). Thickness of cell wall of each isolate was measured from outer cell membrane border to the outer cell wall border.

There are various factors determining the membrane structure and influencing binding, transport of different ionic/ molecular species which include membrane phase state, hydration, electrostatics, dynamics of the constituent molecules etc [19]. Order of the lipids is a parameter that defines different phases of membrane state: i.e. gel (Lb), Liquid order (Lo) and fluidity (La) [19]. The liquid order (Lo) which is responsible for the membrane microdomains presents a higher level of lipid order and microviscosity compared to fluid phase [19]. The resistance towards drugs is also influenced by the host environment, prior exposure to drugs and over expression of different drug efflux pump proteins.

Membrane properties in this study have been defined at different phases of growth and the physical state of the membrane are reflected in the spectroscopic response of the fluorescence probes used. The clinical sensitive isolate showed difference in membrane order as compared to the laboratory isolate due to their prior exposure to

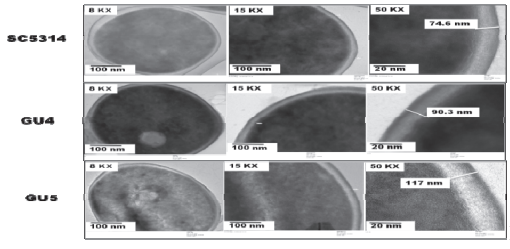

Fig. 3: TEM images of cell envelope of isolates.

variety of host factors and to drugs. The resistant isolate due to over expression of different membrane efflux pump proteins also exhibited different physical state of the membrane. Hence it appears that there are sweet spots in membrane which gradually helps the membrane to acquire a steady state of equilibrium towards the stationary phase of growth. Cell wall thickness observed may be associated to altered cell wall synthesis or may be a non-specific secondary adaptation response linked to change in cell membrane fluidity and/ or function.

This study revealed that membrane fluidity is a parameter of the physical state of the membrane which largely contributes to the passive drug diffusion and observed resistance towards drugs. It of course, merits further investigation to determine if observed differences in cell wall and cell membrane fluidity are strain specific or generalized observations.

Acknowledgements: This work has been supported by grants to TP from Department of Biotechnology (BT/PR5110/MED/29/497/2012 and BT/BI/12/045/2008), University Grants Commission UPE II scheme and Department of Science and Technology (DST-PURSE), India. We acknowledge Joachim Morschhauser, University of Wurzburg for generously providing clinical isolates and expert help of Sobhan Sen, Jawaharlal Nehru University (JNU) for time resolved data analysis. JNU and AIRF for providing infrastructural support and Department of Biotechnology (DBT), India for the award of Senior Research Fellowship to VSR and Junior Research Fellowship to RS are gratefully acknowledged.

References

[1] Odds FC, Brown AJP and Gow NAR. Antifungal agents: mechanisms of action. Trends Microbiol. 2003; 11(6):272-279.

[2] Weig M and Brown AJP. Genomics and the development of new diagnostics and anti *Candida* drugs. Trends Microbiol. 2007; 15(7):310-317.

[3] Mayer FL, Wilson D and Hube B. *Candida albicans* pathogenicity mechanisms. Virulence. 2013; 4(2):119–128.

[4] Liu S, Hou Y, Chen X, Gao Y, Li H, Sun S. Combination of fluconazole with non-antifungal agents: A promising approach to cope with resistant *Candida albicans* infections and insight into new antifungal agent discovery. Int J Antimicrob Agents.2014; 43(5):395–402.

[5] Arendrup MC, Dzajic E, Jensen RH, Johansen HK, Kjaeldgaard P, Knudsen JD, Kristensen L, Leitz C, Lemming LE, Nielsen L, Olesen B, Rosenvinge FS, Røder BL and Schønheyder HC. Epidemiological changes with potential implication for antifungal prescription recommendations for fungaemia: data from a nationwide fungaemia surveillance programme. Clin. Microbiol Infect. 2013; 19(8):343–353.

[6] Cannon RD, Lamping E, Holmes A. R, Niimi K, Tanabe K, Niimi M and Monk BC. *Candida albicans* drug resistance another way to cope with stress. Microbiology. 2007; 153(10):3211–3217.
[7] Kanafani ZA and Perfect JR. Resistance to Antifungal Agents: Mechanisms and Clinical Impact. Clin. Infect Dis. 2008; 46(1):120-128.
[8] Prasad T, Sethumadhavan S and Fatima Z. Altered Ergosterol biosynthetic pathway - an alternate multidrug resistance mechanism independent of drug efflux pump in human pathogenic fungi *C. albicans*. Science against microbial pathogens: communicating current research and technological advances. Formatex Microbiology series. 2011; 3:757-768.
[9] Franz R, Ruhnke M and Morschhauser J. Molecular aspects of fluconazole resistance development in *Candida albicans*. Mycoses. 1999; 42(7-8):453–458.
[10] Fonzi WA and Irwin MY. Isogenic Strain Construction and Gene Mapping in *Candida albicans*. Genetics. 1993; 134(3):717-728.
[11] Prasad T, Chandra A, Mukhopadhyay CK and Prasad R.Unexpected Link between Iron and Drug Resistance of *Candida spp*.: Iron Depletion Enhances Membrane Fluidity and Drug Diffusion, Leading to Drug-Susceptible cells. Antimicrob. Agents Chemother. 2006; 50(11):3597–3606.
[12] Wayne, PA. Reference Method for Broth Dilution Antifungal Susceptibility Testing of Yeasts. Approved Standard M27-A3, third ed. Clinical and Laboratory Standards Institute. CLSI. 2008.
[13] Prasad T, Hameed S, Manoharlal R, Biswas S, Mukhopadhyay CK, Goswami SK and Prasad R. Morphogenic regulator *EFG1*affects the drug susceptibilities of pathogenic *Candida albicans*. FEMS Yeast Res.2010; 10(5):587–596.
[14] Mukhopadhyay K, Prasad T, Saini P, Pucadyil TJ, Chattopadhyay A, and Prasad R. Membrane Sphingolipid-Ergosterol Interactions Are Important Determinants of Multidrug Resistance in *Candida albicans*.Antimicrob. Agents Chemother.2004; 48(5):1778–1787.
[15] Shinitzky M and Barenholz Y. Fluidity parameters determined by fluorescence polarization. Biochim. Biophys. Acta. 1978; 515:367–394.
[16] Verma SD, Pal N, Singh MK and Sen S. Probe position-dependent counterion dynamics in DNA: Comparison of time-resolved Stokes shift of groove-bound to bsae stacked probes in the presence of different monovalent counterions. J PhysChemLett. 2012; 3:2621-2626.
[17] Arora A, Raghuraman H and Chattopadhyay A. Influence of cholesterol and ergosterol on membrane dynamics: a fluorescence approach. BiochemBiophys Res Commun. 2004; 318:920-926.
[18] Mishra NN, Bayer SA, Tran TT, Shamoo Y, Mileykovskaya E, Dowhan W, Guan Z and Arias CA. Daptomycin resistance in Enterococci is associated with distint alteration of cell membrane phospholipids content. PLoS One. 2012; 7(8):e43958:1-10.
[19] Klymchenko AS and Kreder R. Fluorescent probes for lipid rafts: from model membranes to living cells. Chem. Biol. 2014; 21:97-113.

A protocol for screening protein-protein interaction inhibitors with the "Two phages" Two Hybrid assay

L. Grenga[*,1] and **P. Ghelardini**[2]

[1] Laboratory of General Microbiology, Biology Department, University of Rome Tor Vergata, via della Ricerca Scientifica 1 00133 Rome, Italy
[2] Institute of Biology, Molecular Medicine and Nanotechnology of CNR c/o Biology Department, University of Rome Tor Vergata, Rome, Italy
*Corresponding author: e-mail: lucia.grenga@uniroma2.it , Phone: +39 06 72594217

Bacterial cell division is an essential process, interesting for two main reasons: a basic biological knowledge and the possibility to exploit the cell division proteins as primary targets for novel broad-spectrum antibacterial drugs. The "Two phages" two hybrid assay (THA) already used to depict the *E. coli* and *S. pneumoniae* cell division interactome, could constitute a useful tool to select small molecules interfering with the interactions among the division proteins. These molecules, binding to residues involved in protein interactions, on the proteins contact surfaces, could provide both a complementary and more flexible approach for studies on molecular mechanism of cell division and, as important applicative consequence, they potentially constitute a novel class of antimicrobial agents with a very low risk of resistance. At this regard, we set the assay, described in this paper, for the screening of small molecules (or peptides/peptidomimetics) to identify protein-protein interaction inhibitors. This assay, based on the two phages THA, was validated using 3'-(2-phenyl-1H-indol-3-yl)-[1,1'-biphenyl]-3-carboxylic acid, that is known for interfering with the interaction between the *E. coli* division proteins FtsZ and ZipA.

Keywords β-galactosidase activity; Protein-protein interaction; Inhibitors; Lambdoid phage repressors; Small molecules; Two hybrid assay

1. Introduction

Proteins are the main effectors of cellular processes. In fact, most of the cell functions are the result of complex machineries where proteins are organized in dense interaction networks, either stably assembled in multi-protein cellular 'machines' or transiently interacting with one another in a signal transduction cascade.

Among the numerous *in vivo* and *in vitro* approaches described to study the protein interactions, the bacterial "Two phages" two hybrid assay (THA) [1] was successfully used to study the *E. coli* and *S. pneumoniae* division interactome [2], clarifying some of the molecular aspects of prokaryotic divisome formation. The study of bacterial division interaction network shows an important applicative fallout since protein–protein interactions (PPIs) have emerged as promising drug targets. Inhibitors of these interactions could account for the purpose of the modern pharmaceutical research focused on the identification of novel antibacterial agents able to play down the rising of bacterial resistance that, still represents the main problem of antibiotic therapy.

Small molecules that bind to specific residues on the protein contact surfaces [3] could constitute a novel class of antimicrobial agents with a very low risk of resistance. As a matter of fact, impairing the interaction between two proteins A and B forming a heterodimer A-B, essential for the bacterial survival, will be lethal. Bacterial mutants, antiA-B resistant, need a mutation at the interface between antiA-B and A or B protein. These mutants will be also lethal, since the protein, mutated in the interaction site, will be not able to interact with its wild type partner. Only the double mutants, simultaneously mutated in both the two partner proteins, will be selected. This kind of mutants is much less frequent compared to the mutants in the A or B domains, recognized by the old style antibiotics, resulting in a very low rate of bacterial resistance.

At this regard, a screening assay based on the "Two phages" THA, characterized by feasibility, reproducibility and low cost, could constitute a useful tool to identify small molecules that, interfering with the protein interactions, could therapeutically modulate the bacterial cell division**.**

2. Materials and Methods

2.1 Media and chemicals

LB broth for bacterial culture and plating and SM (salt solution) for bacteria dilutions were as described by Miller [8]. The antibiotics, ampicillin (50 μg ml^{-1}), tetracycline (40 μg ml^{-1}) and kanamycin (30 μg ml^{-1}), DMSO and Polymyxin B nonapeptide (PMBN) were purchased by Sigma.

2.2 Bacterial strains and plasmids

Bacterial strains, *E. coli* K-12 derivatives, and plasmids used in this work are listed in Table 1.

2.3 General microbiological and recombinant DNA techniques

Standard microbiological techniques were as described by Miller [4]. Standard procedures were used for small-scale plasmid preparations, agarose gel electrophoresis and bacterial transformation [5]. PCR was carried out using the *Taq* DNA polymerase kit (Promega), according to the recommendations of the manufacturer.

2.4 Assay conditions

The assay derives from the "Two phages" THA, already described [2]. The *E. coli* 7118SB bacterial strain was transformed with the two plasmids pcI_{P22} and pcI_{434} containing the genes coding for the two interacting proteins, against which small molecules as inhibitors were looking for, were under the control of p_{LAC} and p_{ARA} respectively (Figure 1). Clones were selected on LB plates supplemented with the opportune antibiotics and 1% glucose to inhibit the expression from p_{LAC}. Clones were grown in LB in 2 ml wells plate at 37°C to OD_{600} 0.3 (usually it takes about 90 minutes). The culture was then diluted to an OD_{600} of about 0.1 and distributed in aliquots of 200 µl of LB supplemented with 2.5 µg/ml PMBN and IPTG $1x10^{-4}$ M, to induce the expression of one of the two proteins under investigation, in 96 wells plate. At this time (T_0 of the experiment) the inhibitor in DMSO was added to each aliquot. After incubation at 37°C for 30 minutes, L-arabinose 0.2%, to induce the expression of the partner protein, was added and the plate was incubated at 37°C to T=180 minutes. The OD_{600} was determined on aliquots of 100 µl, withdrawn from each well, and the β-galactosidase activity was tested on 50 µl of the remaining culture, as described by Miller [3], lysing the cells with SDS and chloroform. The Miller units of β-galactosidase produced from each culture were normalized with that produced by the 7118SB strain without or harbouring only one plasmid. In the "Two phages" THA, the interaction, and its strength, was calculated from the amount of β-galactosidase produced by the 7118SB strain, harbouring the two plasmids, normalized on that produced by the same strain harbouring only one of the two plasmids. A residual activity less than 50% is indicative of protein interactions [6].

If the interaction between the two proteins, under investigation, was inhibited by an interfering small molecule, the residual β-galactosidase activity will increase from less than 50% up to the 100% value of the reporter strain.

In all the experiments described in this paper, the reported β–galactosidase values were the means of at least four independent determinations where the standard deviation did not exceed ± 4%.

3. Results and discussions

3.1 Setting the assay

Various parameters have been taken into account in order to set a protocol for screening small molecules impairing PPIs with the "Two phages" THA.

a) Bacterial growth in the assay conditions

The assay was set to be performed in 96 well plates. The bacterial growth of strain 7118SB and of its derivatives harbouring the two plasmids pcI_{434} and pcI_{P22}, was examined in a final volume of 200 µl of LB medium, without shaking. In the assay condition, 7118SB strain grew with a generation time of 45 minutes that became 50 and 60 minutes for its derivatives, depending on the proteins cloned in the two plasmids, when their expression was induced with $1x10^{-4}$ M IPTG and 0.2% L-arabinose. Growth saturation was reached early, at $OD_{600} \sim 0.4$ for strain without or harbouring only one plasmid. When both the two proteins forming the chimeric repressor were expressed in the bacterial strain, the growth was blocked at OD_{600} 0.15-0.3, again depending from the expressed proteins. To perform the assay in exponential growth conditions, a pre-culture of the 7118SB strain containing either only one or both plasmids was grown at 37°C in LB to OD_{600} 0.3, then diluted 3 times in LB supplemented with the inducers and let grow for 3 hours. During this period the growth as well as the β-galactosidase synthesis remained exponential (data not shown).

b) Evaluation of both cell wall permeation and concentration of the DMSO on the bacterial growth.

The ability to permeate the *E. coli* bacterial cell, to allow the entry of the small molecules, was tested by evaluating the minimal inhibitory concentration (MIC) of novobiocin in the presence or absence of various amount of Polymyxin B nonapeptide (PMBN), a cationic cyclic peptide derived from the antibacterial peptide Polymyxin B, that specifically increases the permeability of the outer membrane of Gram-negative bacteria toward hydrophobic antibiotics, testing at the same time its effect on cell viability. As expected [7], the MIC of

novobiocin, which was 50 μg/ml in the absence of PMBN, became 6.2 μg/ml in the presence of 2.5 μg/ml of PMBN and this value remained constant increasing the PMBN concentration up to 5 μg/ml and 10 μg/ml. The bacteria growth rate was only slightly reduced with a PMBN concentration of 2.5 μg/ml (<10% increase of the generation time after 3 hours of incubation) whereas with 5 μg/ml the increase of generation time was more than 30%.

Since compounds to be tested should be re-suspended in DMSO, its effects on bacterial growth were also evaluated adding various concentrations to an exponentially growing culture, in the assay conditions. After 3 hours of incubation, the bacterial growth, unaffected in the presence of DMSO ranging from 0 to 2%, decreases of 60% with 5% and of 90% with 10% DMSO.

In conclusion, the assay conditions foresaw the presence of at least 2.5 μg/ml of PMBN to allow the entry of the compounds that should be re-suspended in DMSO in such a way that its final concentration in the bacterial culture should not exceed 2%.

3.2 Effect of 3'-(2-phenyl-1H-indol-3-yl)-[1,1'-biphenyl]-3-carboxylic acid on FtsZ-ZipA interaction

Sutherland et al., [8] described some compounds that can interfere with the interaction between the *E. coli* FtsZ and ZipA proteins, identifying the domain constituted by the last 15 residues of FtsZ as the target of their action. In order to validate our assay for selecting PPIs inhibitors, we studied, in our conditions, the inhibitory action on FtsZ-ZipA interaction of one of these compounds, the 3'-(2-phenyl-1H-indol-3-yl)-[1,1'-biphenyl]-3-carboxylic acid (C27H19NO2), purposely synthetized by "Coliseum Combinatorial Chemistry Centre for Technology (C4T)" (Rome, Italy).

To study the effects of C27H19NO2 on the bacterial growth, we measured its MIC in strain 7118SB. According with Sutherland et al., [8], it was about 300 μM, whereas in the assay conditions, i.e. in the presence of of 2.5 μg/ml PMBN, the MIC was reduced to 20 μM.

a) Study of FtsZ-ZipA interaction in the assay condition

As a first step, we checked whether the assay conditions were suitable to reveal the FtsZ-ZipA interaction. Two sets of plasmid pairs, formed by pcI_{434}*ftsZ* and pcI_{P22}*zipA* and pcI_{434}*ftsZ*$_{15Cter}$ (coding for the FtsZ derivative domain of 15 residues) and pcI_{P22}*zipA*, respectively, were used. In the control strains 7118SB without plasmids, the β-galactosidase produced was on the order of 2000 Miller Units and, as expected, this value did not change in its derivative strain harbouring only the pcI_{434}*ftsZ* plasmid. The β-galactosidase values obtained in the assay, using the strain harbouring both plasmids, were normalized on this value, which constituted the 100% of residual activity (Figure 2). Results indicated that the interaction ability increases as a function of time from 41% of residual activity after 3 hours of induction to 27% after 5 hours, depending on the amount of proteins expressed in the cell upon induction. As shown in Figure 2, both the whole FtsZ protein and its domain $FtsZ15_{Cter}$ behave in the same way as far as the interaction with ZipA is concerned.

b) Inhibition of FtsZ-ZipA interaction with C27H19NO2

Various parameters were taken into account to study the FtsZ-ZipA interaction inhibition with C27H19NO2 by means the "Two phages" THA: (i) the interaction target analysing the inhibitory with both the whole FtsZ protein and its derivative of 15 residues, (ii) kinetics of inhibition, studied at 0, 180 and 300 minutes after the C27H19NO2 addition, with two concentration of the compound, 100 and 300 μM (iii) effect of inhibitor concentration. The kinetics of inhibition was and assays were performed with 0, 10, 25, 50, 75, 100 and 300 μM of C27H19NO2, to determine its minimal and the optimal concentrations to inhibit the interaction. Lastly, (iv) specificity of the inhibitory effect was examined.

(i) As expected, from the data of Sutherland et al., [8], no differences in interaction inhibition were observed performing the assay with both FtsZ and $FtsZ_{15Cter}$ (Figure 3b). (ii) Interaction inhibition due to C27H19NO2 is maximal at T=180 minutes with 100 μM of the compound (Figure 3a). The reduction of the inhibitory effect over this concentration could be due to a precipitation of the compound that is poorly soluble at 300 μM. In every case, it should be taken into account that the inhibitory effect was the result of counterbalance between the C27H19NO2 action and the amount of its target protein interacting with its partner in the cell.

(iii) In Figure 3c, the results of the inhibitory effect as a function of the compound concentration were reported. The maximal activity of C27H19NO2 was observed between 25 and 50 μM where the residual activity of β-galactosidase was of the same order of the control. These concentrations are slightly superior to the minimal inhibitory concentration (MIC), which was 20 μM, in the same experimental conditions.

(iv) Lastly, we analyzed the specificity of C27H19NO2 action studying its effects on three pairs of couples of interacting proteins. Two of them belonged to the *E. coli* division interactome and the third one was formed by the C-terminal part of the 434 phage repressor fused in frame with the N-terminal portions of phages 434 and P22 repressors, respectively, to originate a functional chimeric 434 repressor. The two divisome couples were FtsZ-FtsA, whose interaction is localized at C-terminal of FtsZ protein, involving the same site of FtsZ-ZipA

interaction. Indeed FtsA and ZipA compete for the same site on FtsZ [9]. The second couple was formed by FtsQ and FtsI. This couple of proteins was chosen since none of them interacts with FtsZ [1]. The results of the experiments, reported in Figure 4, showed that the interaction between FtsA and FtsZ was inhibited at the same extent as FtsZ-ZipA. This result could somehow be expected since the same domain of FtsZ is involved in both FtsA and ZipA interactions.

On the other hand, when the 7118SB strain harboured the plasmid pairs coding for either FtsI and FtsQ or for the two subunits of 434 phage repressor, the residual β-galactosidase activity remained almost constant and comparable to that obtained in the absence of inhibitor, despite the presence of increasing amounts of C27H19NO2, highlighting its specific action only on the FtsZ C-terminal domain.

In conclusion, this assay can be used to test ligands with a wide range of size (from 15 to about 400 residues, in the reported case) and proved to be selective and reproducible. Due to its feasibility and operating speed it can be easily adapted for high-throughput drug discovery efforts in the screening of small molecules inhibitors of protein-protein interactions.

Table 1 Bacterial strains and plasmids used in this work

Bacterial strain	Relevant genotype	Source
71/18	SupE thy Δ(lac-proAB9 F' [proAB$^+$ lacI^q lacZDM15]	[10]
7118SB	71/18 *glpT*::O-P434/P22 lacZ	[11]
Plasmids		
$p_{ARA}cI_{434}$	$P_{LAC}cI_{434}$ derivative harbouring the *araC* p_{ARA} region	This work
$p_{ARA}cI_{434}$*ftsZ*	$P_{LAC}cI_{434}$ derivative harbouring the *E. coli ftsZ* gene	This work
$p_{ARA}cI_{434}$*ftsZ*$_{15Cter}$	$P_{LAC}cI_{434}$ derivative harbouring the 15 residues at C-ter of *E. coli ftsZ* gene	This work
$p_{ARA}cI_{434}$*ftsI*	$P_{LAC}cI_{434}$ derivative harbouring the *E. coli ftsI* gene	This work
$p_{ARA}cI_{434}cI_{434Cter}$	$P_{LAC}cI_{434}$ derivative harbouring the C-ter of 434 repressor	This work
$p_{LAC}cI_{P22}$*zipA*	pcI_{P22} derivative harbouring the *E. coli zipA* gene	Our Lab
$p_{LAC}cI_{P22}$*ftsA*	pcI_{P22} derivative harbouring the *E. coli ftsA* gene	Our Lab
$p_{LAC}cI_{P22}$*ftsQ*	pcI_{P22} derivative harbouring the *E. coli ftsQ* gene	Our Lab
$p_{LAC}cI_{P22}cI_{434Cter}$	pcI_{P22} derivative harbouring the C-ter of 434 repressor	Our Lab

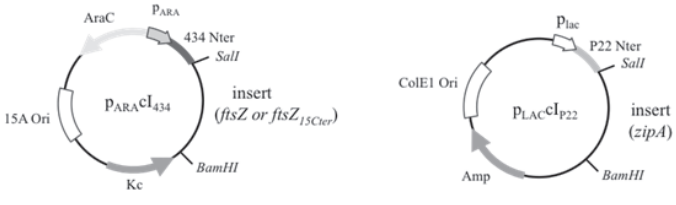

Fig. 1 *Maps of plasmids* $p_{ARA}cI_{434}$*ftsZ and* $p_{LAC}cI_{P22}$*zipA.* Schematic representation of plasmids $p_{ARA}cI_{434}$*ftsZ* and $p_{LAC}cI_{P22}$*zipA*.

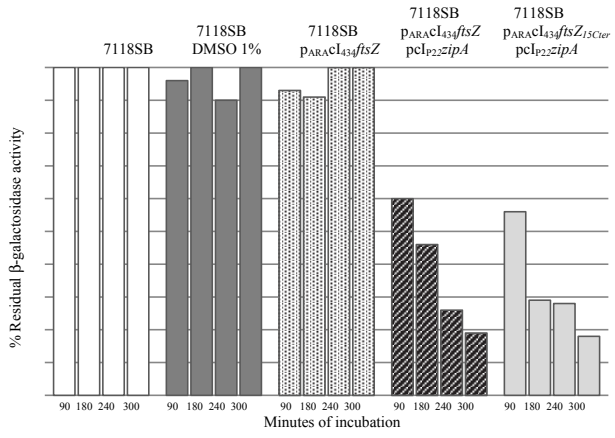

Fig. 2 *Protein interaction in the assay conditions.* Residual β-galactosidase activity measured as function of time in *E. coli* 7118SB strain, supplemented or not with 1% DMSO, and its derivatives containing either the $p_{ARA}cI_{434}$*ftsZ* and $p_{LAC}cI_{P22}$*zipA* plasmids or $p_{ARA}cI_{434}$*ftsZ* $_{15Cter}$ and $p_{LAC}cI_{P22}$*zipA*.

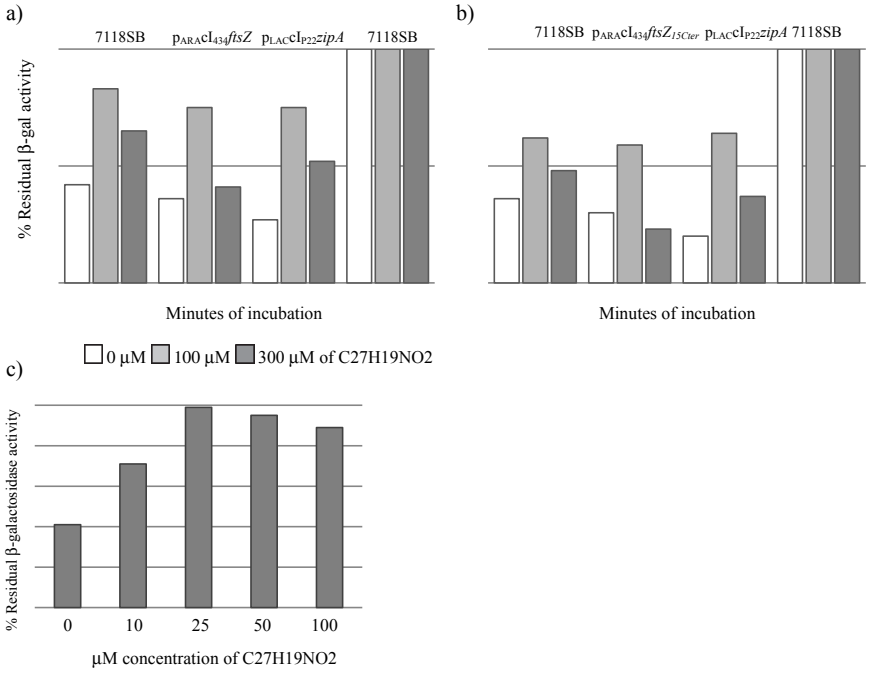

Fig. 3 *Effect of C27H19NO2 on FtsZ (or FtsZ15$_{Cter}$) ZipA interaction.* a) Residual β-galactosidase activity produced by 7118SB strain harbouring $p_{ARA}cI_{434}$*ftsZ* and $p_{LAC}cI_{P22}$*zipA* plasmids or $p_{ARA}cI_{434}$*ftsZ*$_{15Cter}$ and b) $p_{LAC}cI_{P22}$*zipA* as a function of time of incubation with various concentrations of C27H19NO2. c) Residual β-galactosidase activity produced by 7118SB strain harbouring $p_{ARA}cI_{434}$*ftsZ* and $p_{LAC}cI_{P22}$*zipA* plasmids after 3 hours of incubation with various concentrations of C27H19NO2. This figure is also representative of the behaviour of 7118SB strain harbouring $p_{ARA}cI_{434}$*ftsZ*$_{15Cter}$ and $p_{LAC}cI_{P22}$*zipA*.

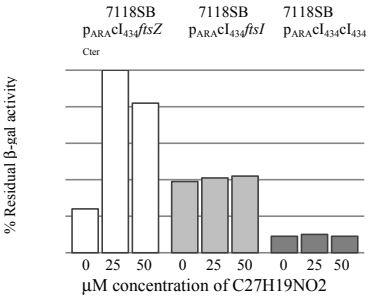

Fig. 4 *Specificity of interaction inhibition with C27H19NO2***.** Residual β-galactosidase activity produced by 7118SB strain harbouring various pairs of plasmids coding for interacting proteins (namely: $p_{ARA}cI_{434}$*ftsZ* $p_{LAC}cI_{P22}$*ftsA*, $p_{ARA}cI_{434}$*ftsI* $p_{LAC}cI_{P22}$*ftsQ* and $p_{ARA}cI_{434}$*cI434Cter* $p_{LAC}cI_{P22}$*cI434Cter)* after 3 hours of incubation with various concentrations of C27H19NO2.

Acknowledgements We are most grateful to C4T for the synthesis of C27H19NO2 and to the Microbiology Laboratory of Angelini ACRAF Pharmaceutical for their support in some experiments. This work was financed by a FILAS biotechnology project and a contract with Angelini ACRAF spa.

References

[1] Di Lallo G, Fagioli M, Barionovi D, Ghelardini P & Paolozzi, L. Use of a two-hybrid assay to study the assembly of a complex multicomponent protein machinery: bacterial septosome differentiation. Microbiology. 2003; 149:3353–3359.

[2] Maggi S, Massidda O, Luzi G, Fadda D, Paolozzi L, & Ghelardini P. Division protein interaction web: identification of a phylogenetically conserved common interactome between *Streptococcus pneumoniae* and *Escherichia coli*. Microbiology. 2008; 154:3042-3052.

[3] Wells JA & McClendon CL. Reaching for high-hanging fruit in drug discovery at protein–protein interfaces. Nature. 2007; 450:1001-1009.

[4] Miller JH. *Experiments in Molecular Genetics*. Cold Spring Harbor, NY: Cold Spring Harbor Laboratory. 1972.

[5] Sambrook, J., Fritsch, E. F. & Maniatis, T. *Molecular Cloning: a Laboratory Manual*. Cold Spring Harbor, NY: Cold Spring Harbor Laboratory. 1989.

[6] Fadda D, Santona A, D'Ulisse V, Ghelardini P, Ennas MG, Whalen MB, & Massidda O. Streptococcus pneumoniae DivIVA: localization and interactions in a MinCD-free context. J Bacteriol. 2007; 189:1288–1298.

[7] Ofek I, Cohen S, Rahmani R, Kabha K, Tamarkin D, Herzig Y, & Rubinstein E. Antibacterial synergism of polymyxin B nonapeptide and hydrophobic antibiotics in experimental gram-negative infections in mice. Antimicrob Agents Chemother. 1994; 38:374-377.

[8] Sutherland AG, Alvarez J, Ding W, *et al.* Structure-based design of carboxybiphenylindole inhibitors of the ZipA-FtsZ interaction. Org Biomol Chem. 2003; 1:4138-4140.

[9] Margolin W. The assembly of proteins at the cell division site. In *Molecules in Time and Space: Bacterial Shape, Division and Phylogeny*, Vicente, Tamames and Mingorance Eds. Kluwer Academic/Plenum Publishers. New York. 2004. p. 79-102.

[10] Messing J, Gronenborn B, Müller-Hill B, & Hans Hopschneider P. Filamentous coliphage M13 as a cloning vehicle: insertion of a HindII fragment of the lac regulatory region in M13 replicative form in vitro. Proc. Natl. Acad. Sci. USA. 1977; 74: 3642-3646.

[11] Barbati S, Grenga L, Luzi G, Paolozzi L & Ghelardini P. Prokaryotic division interactome: setup of an assay for protein-protein interaction mutant selection. Research in Microbiology. 2010; 161:118-126.

Adsorption and biodegradation of reactive orange 16 by *Funalia trogii* 200800 in a biofilm reactor using activated carbon as a supporting medium

Yen-Hui Lin*

Department of safety, Health and Environmental Engineering, Central Taiwan University of Science and Technology, 666 Bu-zih Road, Bei-tun District, Taichung 40601, Taiwan
*Corresponding author: e-mail: yhlin1@ctust.edu.tw, Phone: +886 422391647x6861

A non-steady-state mathematical model system for the kinetics of adsorption and biodegradation by *Funalia trogii* (*F. trogii*) cells on activated carbon was derived. The batch kinetic tests were conducted to determine biokinetic and adsorption parameters. The yield coefficient of *F. trogii* cells obtained from a batch kinetic test was equal to 0.204 mg cell/mg RO16. The maximum specific growth rate (μ_m) of *F. trogii* cells was 0.63 day^{-1}. The maximum specific utilization rate (k) of RO16 was 3.1 mg RO16/mg cell-day. The half-saturation constant of RO16 was 107.3 mg RO16/L. The decay coefficient of *F. trogii* cells was 0.024 day^{-1}. Frundlich isotherm tests were conducted to evaluate the adsorption capacity of activated carbon for RO16. The values for Freundlich isotherm coefficients K_q and n were 0.271 $(g/g)(L/mg)^{1/n}$ and 1.755, respectively. A continuous-flow biofilm reactor using activated carbon as a supporting medium was conducted to evaluate the removal efficiency of RO16. The effluent concentration of RO16 was 0.1-0.2 mg RO16/L. The removal efficiency for RO 16 was approximately 98-99%.

Keywords Adsorption; Biodegradation; Biofilm

1. Introduction

The textile wastewater has a specific characteristic of high temperature, high-alkaline and strong color organic compounds. The color of textile wastewater is various and changeable according to the manufacturing process [1,2]. The treatment of dye wastewater involves chemical and physical methods such as adsorption, coagulation, oxidation, filtration, and ionization radiation. All these methods have different decolorization capabilities, capital cost and operating speed. Among these methods, coagulation and adsorption are the commonly used; however, these created huge amounts of sludge which become a pollutant creating its own disposal problems. Hence, biological processes have received increasing interest as a viable alternative owing to their cost effectiveness, ability to produce less sludge and environmental friendliness [3]. Attempts to develop aerobic bacterial strains for dye decolorization often caused very specific organisms which showed decolorization capability for individual dyes. Additionally, an innovative biological activated carbon (BAC) was developed to allow microorganisms to attach in this study.

2. Model development

The conceptual basis of reactive orange 16 (RO16) from bulk liquid transported into liquid film then diffused into biofilm and activated carbon by intraparticle diffusion is shown in Fig. 1. To model the kinetics of RO16 of adsorption and biodegradation in a completely-mixed reactor, the following assumptions are made [4]: (1) Activated carbon is a homogeneous spherical particle; (2) there is no biological reaction occurred within the activated carbon; (3) A stagnant layer covers the biofilms; (4) no biodegradation occurs inside the activated carbon; (5) local equilibrium occurs at the biofilm- activated carbon interface and (6) the biofilm is homogeneous.

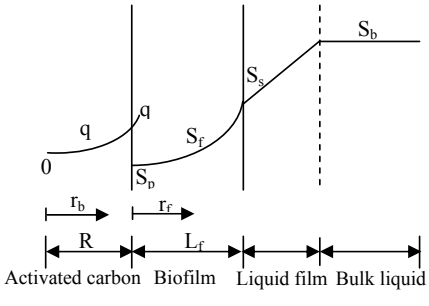

Fig. 1 Concentration profiles for biological activated carbon (BAC)

Two models for intraparticle diffusion are commonly employed: pore diffusion and homogeneous solid diffusion. A homogeneous solid diffusion model, or simply a solid diffusion model, is used in this study. The equation is a typical diffusion equation in spherical coordinates [5]:

$$\frac{\partial q}{\partial t} = \frac{D_b}{r_b^2}\frac{\partial}{\partial r_b}\left(r_b^2 \frac{\partial q}{\partial r_b}\right) \tag{1}$$

where q is the surface concentration of adsorbed RO16 (M_s/M_b); D_b is the surface diffusivity of RO16 (L^2/T); r_b is the radial coordinate in activated carbon (L); and t is time (T).

The RO16 utilization rate by *F. trogii* in the biofilm reactor can be described by the following equation [6]:

$$\frac{\partial S_f}{\partial t} = \frac{D_f}{r_f^2}\frac{d}{dr_f}\left(r_f^2 \frac{dS_f}{dr_f}\right) - \frac{\mu_m}{Y}\frac{S_f}{K_s + S_f} X_f \tag{2}$$

where S_f is the RO16 concentration in the biofilm (M_s/L^3); μ_m is the maximum specific growth rate (1/T); Y is the yield coefficient of *F. trogii* (M_x/M_s); K_s is the half-velocity coefficient of RO16 (M_s/L^3); and X_f is the biofilm density of *F. trogii* (M_x/L^3). The RO16 and *F. trogii* concentrations in the bulk liquid in completely-mixed biofilm reactor can be described as following equations, respectively [6]:

$$\frac{dS_b}{dt} = \frac{Q}{V\varepsilon}\left(S_{b0} - S_b\right) - k_f\left(S_b - S_s\right)\frac{3X_w\left(R + L_f\right)^2}{V\varepsilon\rho_p R} - \frac{kX_b S_b}{K_s + S_b} \tag{3}$$

$$\frac{dX_b}{dt} = \left(\frac{YkS_b}{K_s + S_b} - k_d - \frac{Q}{V\varepsilon}\right)X_b + \frac{3X_w b_s L_f X_f}{V\varepsilon\rho_p R} \tag{4}$$

where S_b is RO16 concentration in the bulk liquid (M_s/L^3); k_d is the decay coefficient (1/T); Q is flow rate (L3/T); V is the effective reactor volume (L3) and ε is the reactor porosity (dimensionless).

3. Materials and methods

The fungal strain *F. trogii* ATCC 200800 is known to be able to degrade various dyes [7]. The fungal strain was grown on potato dextrose agar (PDA) plates at 28°C for 7 days and was stored at 4°C. The experiments were performed not only by cultivation on a solid phase but also by cultivation in liquid. The fungal strain was pre-cultured and it was prepared for the small pieces (the disk size of 1 cm^2 mycelium) on PDA [8,9]. A laboratory-scale completely-mixed biofilm reactor was setup and conducted using RO16 as a model substrate. The bioreactor system consisted of feed tank, pH and DO controllers, a main body of biological activated carbon (BAC) and sampling port. The pure culture of *F. trogii* ATCC 200800 was mixed with the activated carbon before being put into the completely-mixed biofilm reactor. RO16 was measured using UV-vis spectrophotometer (Shimadzu, model UV-1700) at 568 nm [1]. The uninoculated dye free medium was used as blank. All assays were performed in duplicate.

3.1 Supporting media

The specifications of granular activated carbon for G-340 were described as follows: particle size: 8 x 30 mesh; mean particle diameter: 0.9-1.1 mm; hardness: > 93%; bulk density: 0.46-0.50 g/cm^3; total surface area:> 950 m^2/g. Therefore, the total surface area was about 1.92×10^5 cm^2.

3.2 BAC-reactor configuration

The main body of the BAC-reactor with 9 cm in diameter and 132 cm in the bed length is shown in Fig. 2. The BAC-reactor with a high recycle flow rate (Q_r/Q = 20) to maintain a completely nixed column reactor was conducted to evaluate the kinetics of RO16 decolorization by *F. trogii*. The feeding stream containing nutrient medium and reactive-dye substrate (10 mg RO16/L) was continuously pumped upward from the lateral side into the column throughout the distributed plate. The organic loading rate of RO16 was 0.08 kg/m^3-d. Samples were collected from the effluent at the designated time intervals to measure the residual dye concentration and suspended cells concentration. On the bottom of reactor, a sedimentation zone was designed to accumulate decay and shear-off biomasses throughout the entire experiment. The effective volume of reactor is 8.4 L, which yields a hydraulic retention time (HRT) of 3 h. The reactor temperature was controlled at 28°C using an automatic moisture-proof heater. The pH was maintained at 7.3-8.4 and DO was maintained at 7.8-8.2 in the influent throughout the experimental test.

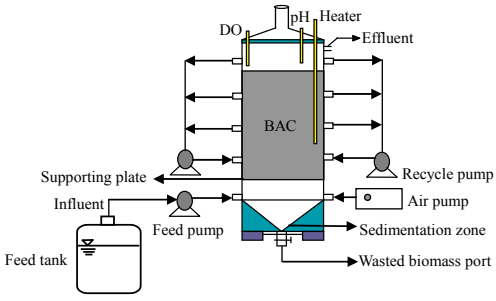

Fig. 2 A laboratory-scale biofilm reactor system.

3.3 Analytical methods

Reactive orange 16 was measured using UV-vis spectrophotometer (Shimadzu, model UV-1700) at 568 nm [1]. The uninoculated dye free medium was used as blank. All assays were performed in duplicate and compared with uninoculated controls. Viable cells were counted by using serial dilution technique and confirmed by plating on nutrient agar and incubated at 28°C for about 24 h to determine *F. trogii* cells concentration.

4. Results and discussion

4.1 Biokinetic and reactor parameters

The input parameters to the model for RO16 decolorization by *F. trogii* in BAC-process were listed in Table 1. The parameters are categorized as follows: (1) measured by kinetic tests; (2) calculated from empirical formula listed in literature; (3) assigned as needed to fit the experimental data.

Table 1 Input parameters to kinetic BAC-model system

Parameter	Symbol	Value	Unit
Measured			
RO16 concentration in the feed	S_{b0}	10	mg RO16/L
Freundlich isotherm coefficient	n	1.755	dimensionless
Freundlich isotherm coefficient	K_p	0.271	$(g/g)(L/mg)^{1/n}$
Maximum specific utilization rate of RO16	k	3.1	mg RO16/mg cell-day
Half-velocity coefficient of RO16	K_s	107.3	mg/L
Yield coefficient of *F. trogii* cells	Y	0.202	mg cell/mg RO16
Decay coefficient of *F. trogii* cells	b	0.024	day^{-1}
Concentration of suspended *F. trogii* cells in the feed	X_{b0}	4.8×10^{-3}	mg/cm^3
Surface diffusivity of RO16	D_s	6×10^{-4}	cm^2/day
Influent flow rate	Q	6.7×10^{4}	cm^3/day
Effective reactor volume	V	8.4×10^{3}	cm^3
Total surface area of activated carbon	A	1.92×10^{5}	cm^2
Reactor porosity	ε	0.54	dimensionless
Radius of activated carbon particle	R	0.05	cm
Apparent activated carbon density	ρ_p	0.48	g/cm^3
Weight of activated carbon	X_w	$1.54x10^{3}$	g
Calculated			
Liquid film transfer coefficient	k_f	346.8	cm/day
Diffusion coefficient in the biofilm	D_f	0.192	cm^2/day
Shear-loss coefficient of biofilm	b_s	0.253	day^{-1}
Density of *F. trogii* biofilm	X_f	10.64	$mg\ cell/cm^3$
Assigned			
Initial *F. trogii* biofilm thickness	L_{f0}	$5.5x10^{-4}$	cm

4.2 Reactive orange 16 decolorization

The model-predicted and experimental results for decolorization of RO16 are shown in Fig. 3(a). The RO16 concentrations are all normalized with respect to the influent substrate concentration. The model simulated the experimental results fairly well throughout the entire course of the test. The substrate concentration first increased steadily to about 0.6 mg/L (0.06 S_{b0}) at 0.2 days. At this period of time, there was no significant biological growth inside the reactor and no detectable biodegradation of the RO16 by *F. trogii* in the reactor. The reactor was behaving similar to an activated-carbon-adsorber, and the substrate-concentration curve was the same as a typical breakthrough curve of an activated carbon adsorber. At this stage, activated carbon was adsorbing substrate without significant resistance to the diffusion of the RO16 posed by the *F. trogii* biofilm. The second part of the RO16 curve ran from 0.2 days to 2 days, when the RO16 curve started to deviate from the breakthrough curve of a carbon adsorber. The effluent concentration of RO16 decreased rapidly. Apparently, attached and suspended *F. trogii* cells were actively utilizing the RO16 during this period. Meanwhile, attached and suspended *F. trogii* cells were actively growing at this time. The model was able to predict reactor performance fairly well during this transient period. The third part of the substrate curve ran from 2 days to 4 days. At this period, the experimental data were lower than modeling results for the effluent of substrate. The reason was that the microorganisms grew enough to form biofilm. Thus, the effect of shear loss became insignificant although biofilm became thicker. The lower shear loss results in lower suspended biomass. The suspended cells decomposed and released soluble microbial products (SMP) was insignificant in the effluent concentration of RO16 at this period of time. The fourth part of the substrate curve ran from 4 days to 7.9 days. At this period, the BAC-process reached a steady-state condition and the effluent of substrate was about 0.2 mg/L (0.02 S_{b0}). The removal efficiency for substrate was about 98% at this period. As can be seen, the model prediction is in fair agreement with the experimental result. Although the soluble microbial products (SMP) would be released by biofilm at this stage, the SMP produced by the biodegradation of RO16 would be adsorbed by activated carbon, which made SMP not a significant interference to the effluent.

4.3 Growth of suspended cells

Fig. 3(b) shows the generating suspended biomass varied with time. The growth concentration curve went through log-growth phase then reached a steady-state condition. The elapsed time required for suspended *F. trogii* cells to reach a steady-state condition is almost the same with that for substrate biodegradation. This indicated that the suspended *F. trogii* cells reached a maximum growth rate while substrate had a maximum utilization rate at a steady-state condition. The maximum growth at steady-state condition was maintained at 18.6 mg cell/L.

4.4 Flux into biofilm and activated carbon

There are two fluxes of RO16 in the BAC-process; the flux from the liquid phase into the *F. trogii* biofilm (J_b) and the flux from the *F. trogii* biofilm into the activated carbon (J_p). J_b and J_p varied with time in the BAC-reactor are plotted in Fig. 3(c). The figure shows that J_b and J_p were equal at the beginning of the test because the utilization of *F. trogii* biofilm was negligible at this time. Most of the RO16 was decolorized by activated carbon adsorption. The two curves started to deviate with one another around 0.2 days, when the *F. trogii* biofilm started to grow actively. The J_b value for BAC-model started out at a value of 0.08 mg/cm^2-day that was controlled by adsorption when the utilization of *F. trogii* biofilm was zero initially.

J_p in the BAC reactor decreased first due to the fast utilization of the RO16 by the *F. trogii* biofilm, which was beginning to develop. As the *F. trogii* biofilm accumulated, J_p decreased to zero and then went negative, which signaled bioregeneration. The flux J_p changed from a positive value to a negative value at 0.8 days. This required a reversal of the adsorbate density gradient inside the activated carbon. The resulting negative adsorbate density gradient caused the substrate to diffuse out the activated carbon because of the growth of biofilm. As the biofilm grew thicker, the biofilm consumed RO16; thus, the concentration of RO16 at the biofilm/activated carbon interface became lower. As bulk and biofilm concentration declined, they became lower than the concentration at equilibrium with the previously adsorbed substrate. At this point, RO16 simply diffused out of the activated carbon and activated carbon was bioregenerated by the *F. trogii* biofilm. As the steady-state approached, J_p went to 0 asymptotically from a negative value, while J_b approached a constant value. The curves showed that *F. trogii* biofilm utilization became the dominant mechanism responsible for the RO16 removal at steady-state in the BAC-reactor.

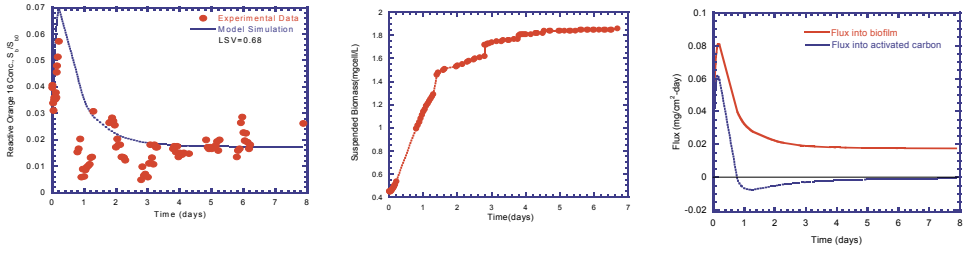

Fig. 3 Experimental data and model simulation (a) RO16 effluent concentration (b) suspended *F. trogii* cells concentration in effluent and (c) Flux into biofilm and activated carbon

5. Conclusions

This study demonstrates the feasibility of using *F. trogii* biofilm and suspended *F. trogii* cells for continuous decolorization of dye-laden influents using BAC-process. The kinetic BAC-model and experimental approaches elucidated the total mechanisms governing the interactions of the activated carbon adsorption and biofilm biodegradation for reactive-dye decolorization by *F. trogii* cells. The BAC-model was able to predict performance fairly well for a non-steady-state experiment. The *F. trogii* Biofilm bioregenerated the activated carbon by lowering the RO16 concentration at the biofilm/activated carbon interface. The RO16 previously adsorbed inside the activated carbon simply desorbed out of the activated carbon through a reversal of flux entering activated carbon. The approaches of experiments and kinetic model presented in this paper can be employed for the design of a pilot-scale or full-scale BAC-process for reactive-dye decolorization by *F. trogii* cells in textile wastewater.

Acknowledgements This research was supported in part by a grant from the Ministry of Science and Technology of Taiwan under Contract No. NSC 100-2221-E-166-004-MY2.

References

[1] Park C, Lee M, Lee B, Kim SW, Chase HA, Lee J, Kim S. Biodegradation and biosorption for decolorization of synthetic dyes by *Funalia Trogii*. Biochemical Engineering Journal. 2007; 36:59-65.
[2] Choi HD, Shin MC, Kim DH. Removal characteristics of reactive black 5 using surfactant-modified activated carbon. Desalination. 2008; 223:290-98.
[3] Rao KR, Srinivasan T, Venkateswarlu Ch. Mathematical and kinetic modeling of biofilm reactor based on ant colony optimization. Process Biochemistry. 2010; 45:961-72.
[4] Liang CH, Chiang PC, Chang EE. Modeling the behaviors of adsorption and biodegradation in biological activated carbon filters. Water Research. 2007; 41:3214-50.
[5] Smith E, Ghiassi K. Chromate removal by an iron sorbent: mechanism and modeling. Water Environment Resesrch. 2006; 78:84-93.
[6] Tsai HH, Ravindran V, Pirbazari M. Model for predicting the performance of membrane bioadsorber reactor process in water treatment applications. Chemical Engineering Science 2005; 69:5620-36.
[7] Arora DS, Chander, M, Gill PK. Involvement of lignin peroxide, manganese peroxide and laccase in degradation and selective of wheat straw. International Biodeterioration & Biodegradation. 2002; 50:115-20.
[8] Kapdan IK, Kargi F, McMullan G, Marchant R. Effect of environment conditions on biological decolorization of textile dyestuff by *C. versicolor*. Enzyme and Microbial Technology. 2000; 26:381-7.
[9] Jang MY, Ryul WR, Cho MH. Laccase production from repeated batch cultures using free myxerlia of *Trametes* sp. Enzyme and Microbial Technology. 2002; 30:741-6.

Antibacterial activity of an aromatic plant from Algerian kitchen

A. Attou[*,1], A. Benmansour[1], F. Haddouchi[1] and **I. Amrani[2]**

[1]Laboratory: Natural Products: biological activities and synthesis (LAPRONA). Faculty of Sciences of Nature and Life & Sciences of Earth and Universe, Department of Biology. University Abou Bekr Belkaid, B.P.119 Tlemcen, 13000, Algeria.
[2] Laboratory ToxiMed, Faculty of Sciences of Nature and life & Sciences of earth and Universe, University Abou Bekr Belkaid, B.P.119 Tlemcen, 13000, Algeria.
*Corresponding author: e-mail: heyfraise21@yahoo.fr, Phone: +213552562910

Ruta chalepensis L. is an aromatic plant belonging to the family of *Rutaceae*, commonly called by locals "Fidjel". It is spontaneous, largely spread in North Africa, especially Algeria.
The rue is a medicinal aromatic plant still used in traditional medicine in many countries as a laxative, anti-inflammatory, analgesic, antispasmodic, abortifacient, antiepileptic, emmenagogue and for the treatment of skin diseases, and very used in many dishes from the aromatic oil and cheese to flavoring any kind of prey.
The extraction by hydrodistillation of the essential oil of the whole aerial plant has significant returns up to 1,90%.
The essential oil has a medium antibacterial activity against staphylococci and streptococci, and no activity or very low against enterobacteriaceae species.

Keywords: bioactive molecules; essential oil; antimicrobial activity; *Ruta chalepensis*.

1. Introduction

Since time immemorial, Men appreciate the soothing and analgesic virtues of plants.

The active principles of medicinal plants are often related to the products of secondary metabolism. Their properties are currently recognized and for a good number listed, and thus harnessed, in the context of traditional medicines and also in modern allopathic medicine [1, 2, 3].

The family *Rutaceae* consists of 150 genera and 1500 species of treelets known to accumulate essential oils, flavonoids, coumarins, and several sorts of alkaloids.

Ruta chalepensis (fig n°1), herbaceous plant with woody stem at the base, can reach 1 m in height, with aromatic foliage, and dark yellow flowers, with four or five petals; it is an ornamental plant in gardens.

The name *Ruta* comes from the greek « rhyté » which means rescued, prevent, or "REO" means flowing certainly making reference to its emmenagogue properties [2,4], and commonly known by the RUE.

In cooking, it is used to flavor sauces and prey, cheese, oil and vinegar [4, 5, 6],

It was used as emmenagogue and abortifacient, it has a clear stimulating effect on the uterus, until today it is so used as : Analgesic; Anti-inflammatory; antiseptic; antispasmodic; aphrodisiac; cardiotonic; sedative; stomachic; the aqueous extracts of the plant has a hypotensive activity by a direct effect on the cardiovascular system [7, 8].

2. Materials and methods

2.1. Plant material

The aerial parts of the plant were collected at flowering season from a station in west Algeria, and then dried at room temperature for two weeks.

Fig n°1: *Ruta chalepensis*

2.2. The extraction of essential oil

It was done by steam distillation of the aerial part of the plant, where 100 g of dry plant is introduced into a flask bi collar, and moistened with water; the mixture is brought to a boil for 2-3 hours. The water laden vapours of essential oil, the refrigerant passing through, condense and drop into a separator funnel; water and oil separate by density difference [1, 9]. The essential oil is stored in dark vials until use.

2.3. Evaluation of the antimicrobial activity

NCCLS, 1990 [10], the activity of essential oils of *Ruta chalepensis* was evaluated by the method of discs on agar, which is a qualitative technique based on measuring the diameters of inhibition in mm.

The antimicrobial activity was evaluated against a sample of wild strains (sample of 131 strains: 101enterobacteriaceae, 14 staphylococci and 16 streptococci) from the Laboratory of Microbiology at the Regional Military University Hospital of Oran during 2 months from 05/01/2014 to 06/03/2014.

The culture of the strains is measured par turbidity; and adjusted to 0.5 standard of McFarland scale, corresponding to 1-2 x 10^8 CFU/ml.

100µl of the suspension used to inoculate the agar plates, then filter paper discs impregnated with the essential oil are disposed, the Petri dishes are incubated at 37°C for 24h (fig n°2).

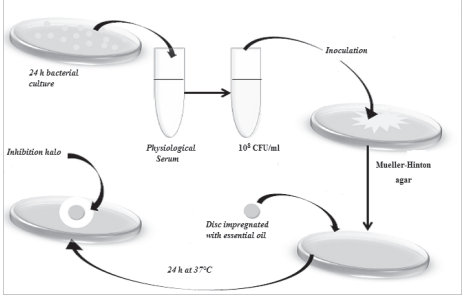

Fig n°2: Evaluation of the antimicrobial activity

3. Results

3.1 Essential oil isolation

The dried aerial parts of the plant subjected to a hydrodistillation have revealed a yield of about 1.90±0.01% (w/w).

3.2 Antimicrobial activity

Table 1 shown the diameters of inhibition of the essential oil against the bacteria tested. The results indicate that the essential oil of *Ruta chalepensis* has low antibacterial activity against all strains; with inhibition zones don't exceed the 15 mm, and no activity against the enterobacterial species.

Table 1 In vitro antibacterial activity of *Ruta*'s essential oil.

Strains	Sample number	Inhibition diameter (mm)		
		6	7-10	10-15
Pseudomonas aeruginosa	13	13	0	0
Escherichia coli	49	47	2	0
Enterobacter cloacae	5	5	0	0
Proteus mirabilis	11	11	0	0
Klebsiella pneumoniae	14	14	0	0
Acinetobacter baumanii	9	9	0	0
Staphylococcus aureus	14	5	3	6
Streptococcus sp.	16	4	5	7